Desalination and Water Treatment
www.deswater.com

doi:10.5004/dwt.2018.22126

105 (2018) 152–159
February

Numerical analysis of the energy recovery process in a disc-type pressure exchanger with pressure-boost effect

Zheng Cao[a], Jianqiang Deng[a,*], Zhihua Chen[b], Wenjun Yuan[a]

[a]*School of Chemical Engineering and Technology, Xi'an Jiaotong University, Xi'an 710049, Shaanxi, China, email: czczkok@stu.xjtu.edu.cn (Z. Cao), Tel. +86 29 82663413, Fax +86 29 82663413, email: dengjq@mail.xjtu.edu.cn (J. Deng), email: yuanwenjun.347@stu.xjtu.edu.cn (W. Yuan)*
[b]*School of Mechanical and Power Engineering, Shanghai Jiaotong University, 200240, Shanghai, China, email: zh03.chen@sjtu.edu.cn (Z. Chen)*

Received 15 September 2017; Accepted 24 January 2018

ABSTRACT

Pressure exchanger acts as an intermediary device that transfers pressure energy between liquid streams in different pressures. This work is an exploratory study to introduce a novel disc-type pressure exchanger, which combines characteristics of both positive displacement and centrifugal type pressure exchangers. In order to properly describe the complex flow behaviors in the rotating disc channels, a three-dimensional numerical simulation was carried out to study the pressure exchange process between brine and seawater streams in the device. The pressure exchange performance including pressure recovery efficiency and mixing rate were evaluated under different operating conditions. Additionally, unbalanced operating methods were discussed for mixing control. Simulation results show that the mixing rate and pressure exchange efficiency of such device are well competent for energy recovery process. And the mixing rate can be further controlled by decreasing flow rate and increasing rotational speed and unbalanced lead flow ratio.

Keywords: Pressure exchanger; Energy recovery; Mixing; Numerical simulation

1. Introduction

With the development of human society and large energy consumption, energy saving becomes an issue of concern. In analogy to heat exchange, there also exists large amounts of pressure that can be utilized in many process fluids. Pressure exchanger is a device that can transfer pressure between different flow streams, and is becoming a core component in various seawater reverse osmosis (SWRO) processes to recover pressure from the membrane reject flow. It is reported that the use of pressure exchanger enables 1.5–27% savings on the high-pressure pump's total energy consumption [1]. Based on the operating principle, pressure exchangers can be classified into centrifugal type and positive displacement type. Typical devices of the former class include Francis turbine, Pelton turbine and hydraulic turbocharger (HTC). Their maximal pressure exchange efficiency ranges from 0.78 to 0.81 [2] because of the secondary conversion in pressure-mechanical energy-pressure process. Examples of the latter class of pressure exchangers are (Calder®) DWEER work exchanger and rotary pressure exchangers (RPE) such as (ERI®) PX pressure exchanger and (Danfoss®) Isave pressure exchanger. The isobaric process benefits such exchangers with up to 0.96 pressure exchange efficiency by direct contact of flows [3]. Since rotary pressure exchanger has no valve controlled system, it switches pressure transfer process with rotating duct channels. As a result of direct contact between fresh seawater and high concentrate brine, mixing becomes inevitable due to the lack of a reciprocating physical piston in the ducts. A 2.5% salinity increase in the fluids at SWRO membrane will lead to an increase of operating pressure by 0.13 MPa [3]. Therefore, mixing control is an important task during RPE operation.

*Corresponding author.

Zhou et al. [4,5] performed numerical simulations of mixing formation in RPE, and investigated the effects of rotor parameters, rotational speed, flow rate on the maximum flow-in length and mixing performance. It is found that volumetric mixing ratio increases with flow rate and decreases with rotational speed. Based on oscillating flow behaviors, Mei et al. [6] performed a theoretical analysis to evaluate the mass transfer process of salt in ducts of RPE, the high efficiency and low mixing rate of isobaric pressure exchanger was theoretically confirmed. Xu et al. [7] carried out a numerical research on a four ports RPE, the relationship between mixing and dimensionless inflow length is in good agreement with experimental result. In addition to the traditional RPE structure, several design improvement features have been proposed. Wang et al. [8] employed pre-pressurization/depressurization grooves on the RPE, and the effects on diminishment of flow fluctuation amplitude were investigated. Cao et al. [9] introduced an RPE with an extended angle on end cover inlet, and its benefit in mixing control was studied by numerical analysis. Al-Hawaj [10] introduced an RPE containing sliding ball pistons as a physical barrier to achieve a no-mixing condition in ducts of RPE. Besides, he also developed a sliding vane work exchanger, which is an ingenious structure similar to the sliding vane compressor, a theoretical analysis and a parametric study were performed thereafter [11]. Since sliding components are introduced in these rotary positive displacement exchangers, abrasion and friction loss may be increased.

Pressure exchange technology is essential in energy saving and promising in various membrane processes. The application of RPE can be extended to more application fields because of its outstanding advantages. The development of RPE configurations are mostly focused on achieving a higher-capacity [12]. However, there is no obvious change in the primary structure. And the pressure exchange process is still based on an isobaric process, where pressure at high-pressure seawater outlet is always lower than high-pressure brine inlet. This work presents a novel disc-type pressure exchanger, which combines characteristics of both positive displacement type and centrifugal type pressure exchangers. This introduced disc-like pressure exchanger can achieve a pressure-boost effect to break the constraint of isobaric pressure exchange process. Pressure exchange performance including pressure exchange efficiency, pressure ratio and mixing rate were numerically evaluated under different operating conditions. Additionally, unbalanced operating methods were discussed for mixing control.

2. Simulation of pressure exchange process in DPE

2.1. Geometric models

In the conventional energy recovery process of the SWRO system, a circulation pump is often used to boost the seawater outflow pressure to drive the flow throughout the system. As shown in Fig. 1, the feed seawater is driven by the high-pressure pump to overcome the osmotic pressure of the RO membrane, part of the flow permeates through the membrane as the pure water, the rest rejection flow with high pressure enters energy recovery device. Due to the advantage of the pressure-boost effect, the application of DPE is expected to avoid the installation of circulation pump in the recovery loop, which makes the system more compact and simple to operate.

The schematic view of DPE presented in our work is illustrated in Fig. 2. In contrast to the conventional axial rotor configuration, the DPE comprises a rotary disc with channels radial-arrayed along the circumference, and two end covers connected to the channel ends. The rotor is externally driven by a motor so that a stable rotation can be adjusted under various operating conditions. Because of the long circumferential length, each end cover contains 4 center-symmetric ports to complete the pressure exchange process twice in each circle.

The number of channels N is set as 60, and the length L and height H of rotor channel are 250 mm and 40 mm respectively. With the continuous rotation of duct channels, the low-pressure fluid flows from LP inlet and is pressurized through the direct contact with the high-pressure fluid from HP inlet. After the pressure recovery process is accomplished, the rest fluid in ducts will be discharged when exposed to the LP outlet.

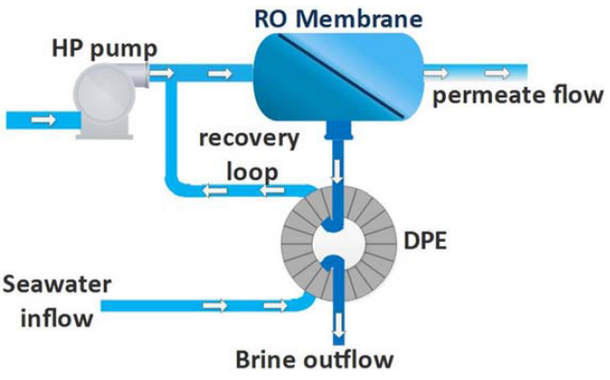

Fig. 1. Schematic view of the single stage SWRO desalination process with DPE.

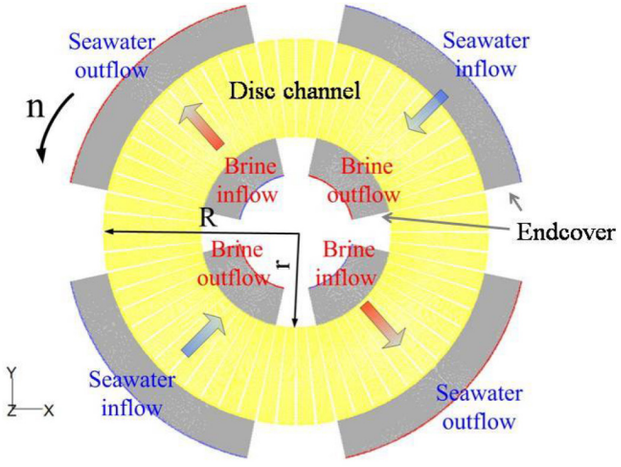

Fig. 2. Schematic view of the DPE.

2.2. Governing equations

The model of the unsteady flow is built based on conservation laws and species transport equation.

Continuity equation:

$$\frac{\partial \rho}{\partial t} + \nabla(\rho \vec{v}) = 0 \tag{1}$$

Momentum equation:

$$\frac{\partial}{\partial t}\left(\rho \vec{v}\right) + \nabla\left(\rho \vec{v}\vec{v}\right) = -\nabla P + \nabla \cdot (\bar{\bar{\tau}}) + \rho \vec{g} \tag{2}$$

Specifies transport equation:

$$\frac{\partial}{\partial t}(\rho \gamma_i) + \nabla \cdot \left(\rho \vec{v} \gamma_i\right) = -\nabla \cdot \vec{J}_i + R_i \tag{3}$$

where the mass diffusion flux can be described as:

$$\vec{J}_i = -\left(\rho D_i + \frac{\mu_t}{S_{C_t}}\right)\nabla Y_i \tag{4}$$

In the above equations, ρ is the density; t is the time; v is the velocity; g is the gravitational acceleration; p is the static pressure; τ is the stress tensor, Y_i is the mass fraction of species i; R_i is the additional source term; D_i is the mass diffusion coefficient for species in the mixture, and S_{ct} is the turbulent Schmidt number.

For turbulent flows, we use standard k–ε model as the turbulence model to close the equations:

$$\frac{\partial}{\partial t}(\rho k) + \frac{\partial}{\partial x_i}(\rho k u_i) = \frac{\partial}{\partial x_j}\left[\left(\mu + \frac{\mu_t}{\sigma_k}\right)\frac{\partial k}{\partial x_j}\right] + G_k + G_b - \rho\varepsilon - Y_M + S_k \tag{5}$$

$$\frac{\partial}{\partial t}(\rho \varepsilon) + \frac{\partial}{\partial x_i}(\rho \varepsilon u_i) = \frac{\partial}{\partial x_j}\left[\left(\mu + \frac{\mu_t}{\sigma_\varepsilon}\right)\frac{\partial \varepsilon}{\partial x_j}\right] + C_{1\varepsilon}\frac{\varepsilon}{k}\left(G_k + C_{3\varepsilon}G_b\right) - C_{2\varepsilon}\rho\frac{\varepsilon^2}{k} + S_\varepsilon \tag{6}$$

where u_i is the time mean velocity, σ_k and σ_ε are Prandtl numbers, G_k and G_b are the turbulent kinetic energies due to the mean velocity gradients and buoyancy respectively, Y_m is the contribution of the fluctuating dilatation in turbulence. S_k, S_ε are the source terms, and the model constant $C_{1\varepsilon}$, $C_{2\varepsilon}$ and $C_{3\varepsilon}$ are set as 1.44, 1.92 and 1.0 respectively.

2.3. Numerical method

The mesh of the simulation domain is shown in Fig. 3, which contains 657,800 structured hexahedral elements. The mesh quality is often examined by the orthogonal quality, which ranges from 0 to 1, and a higher value corresponds to a high mesh quality. In this work, the minimum orthogonal quality is 0.9993, indicating a good mesh quality.

In order to achieve a mesh independent solution, a sensitivity analysis on three meshes, namely 200,116, 657,800 and 1,213,100 cells were performed. The NaCl concentration at a steady state of the three meshes cases are 0.03568, 0.03561, 0.03562 respectively. As almost identical result is found after refining the mesh density, the grid number of 657,800 is used in the simulatuon to save computional power. To run unsteady simulation under various rotational speed, the time step corresponding to 1 degree of angular rotation is applied. Also, a time step independent test was also carried out to verify the sufficiency. As no significant difference in the stable concentration value is found when using a time step size half as large, a time step of 1 angular rotation is used for simiulation which is considered to be computationally efficient.

The commercial software in the mesh generation is GAMBIT, and ANSYS FLUENT 14.5 is used to solve the governing equations in a control volume discretization method. The moving mesh method is applied to the rotor domin at a constant rotational speed. Pressure outlet conditions and velocity inlet conditions are used on outward ports of end covers correspondingly. The inward ports of end covers and duct ends are assigned with interface conditions. The computation conditions for the standard case are given in Table 1.

3. Results and discussion

3.1. Mixing performance

Volumetric mixing rate is used to evaluate the mixing performance of pressure exchanger, and it is defined as:

$$V_m = \frac{c_{so} - c_{si}}{c_{bi} - c_{si}} \tag{7}$$

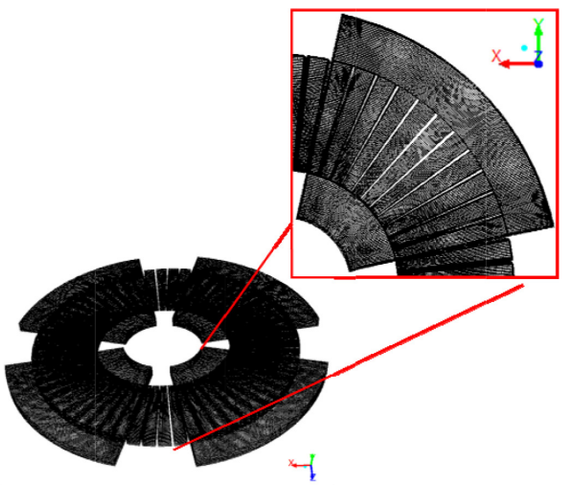

Fig. 3. Mesh of the simulation domain of DPE

Table 1
Simulation condition arrangements for the standard case

Rotational speed (rpm)	500
Inflow velocity ($m \cdot s^{-1}$)	3
Flow rate ($m^3 \cdot h^{-1}$)	590
Operation pressure (MPa)	0.6–6
Species concentration	0.35–0.65

where *c* is the species concentration, the subscript *so*, *si*, *bi* and *bo* refers to high pressure seawater outlet, low pressure seawater outlet seawater inlet, high pressure brine inlet and low-pressure brine outlet respectively.

The mixing formation process can be divided into three stages as is shown in Fig. 4. At time zero, all duct channels are filled with low pressure seawater and the disc starts to rotate. This is the initial stage I. Once the mixing is detected at HP outlet, stage I proceeds to the mixing formation stage II. The mixing rate continuously increases in this stage due to the periodic contact between high pressure brine and low pressure seawater. When the concentration of Nacl at HP outlet becomes gradually stable, and the rate of change is smaller than 1E-4, the steady stage III is considered to be achieved. In this stage, the mixing zone reciprocates in duct channels, separating flows with different concentrations as a liquid piston, resulting in a basically constant concentration of salt at the outlet of DPE. The contours of concentration of high-pressure flow at each state are shown in Fig. 5. It is seen that the distribution of NaCl tends to be stable in both ducts and endcovers after the steady stage.

The operating conditions have a great effect on mixing performance of DPE. The two most important factors are flow rate and rotational speed. It is noted that for flow-driven type pressure exchangers, the rotational speed is mainly determined by inflow velocity. However, it still can be advantageously controlled by means of external force for a better performance [13].

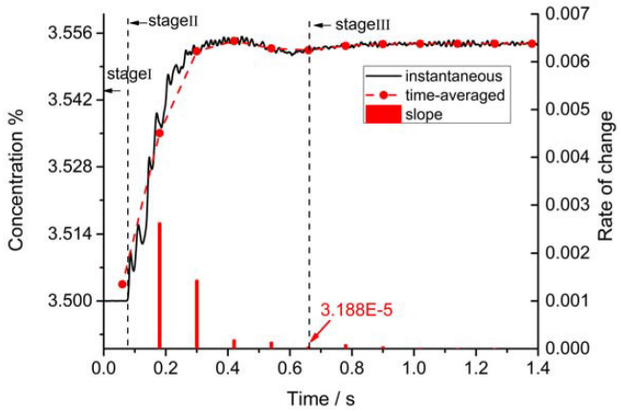

Fig. 4. Mixing formation of DPE at the standard simulation case.

Fig. 6 shows the relationship between flow rate and the volumetric mixing rate at the steady state. With the increasing of flow rate, the mixing rate increases almost proportionality. It is seen that a severe mixing rate of up to 7.69% achieves when the inflow velocity reaches to 7 m/s, the dramatic increase in slope of the curve indicates the mixing zone reached to the ends of duct channels, and a part of liquid piston is probably pushed out by high pressure brine. At a given rotational speed, there exists a limit range in the operating inflow velocity, which is consistent with the rotor in flow height theory in literature [14].

The rotational speed of DPE also has an obvious effect on mixing performance. In our simulation cases, rotational speed varies from 300 to 1500 round per minute, and the trend observed in Fig. 7 is opposite to the trend of mixing rate versus flow rate. At a low rotational speed, the mixing rate is relatively high. As the rotational speed increases, the mixing rate is significantly decreased, and the decline amplitude becomes smaller when the rotational speed is larger than that of 500 r/min. This implies that liquid piston reciprocates in a stable range and the mixing zone has been effectively controlled at a higher rotational speed.

Mixing in DPE is mainly caused by mass diffusion and convention, and convention is likely a dominant factor in

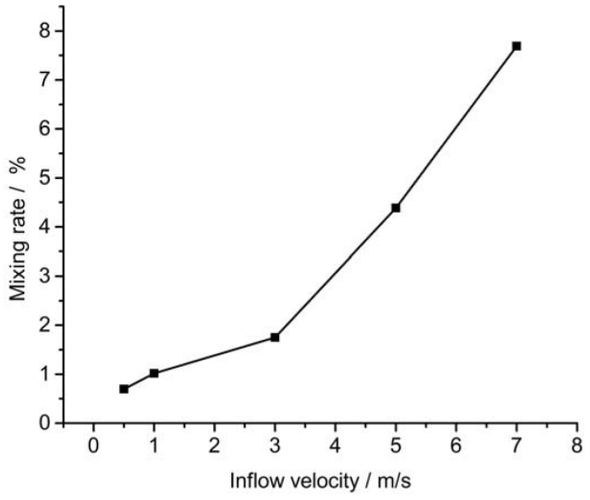

Fig. 6. Volumetric mixing rate varies with inflow velocities at a rotational speed of 500 r/min.

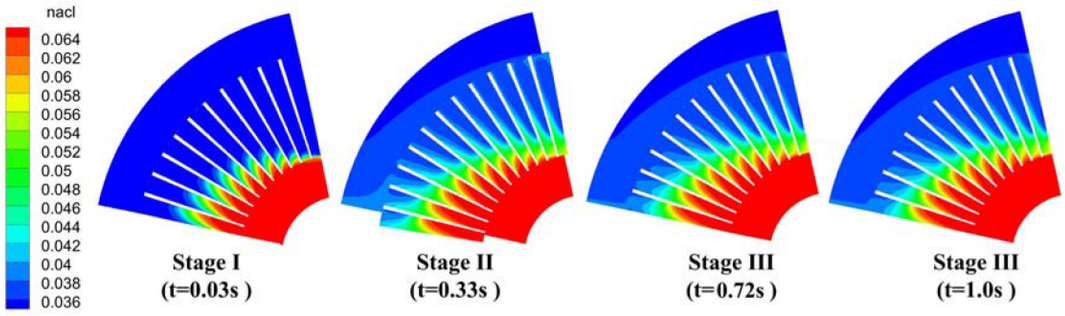

Fig. 5. Concentration field of NaCl on plane of z/H = 0.5 in high- pressure region at different stages.

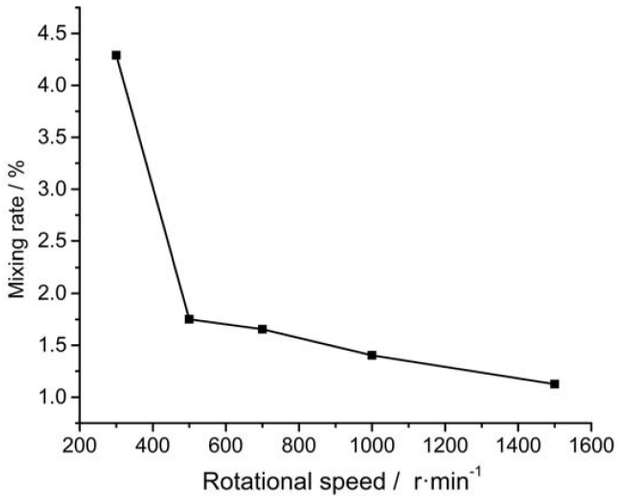

Fig. 7. Volumetric mixing rate varies with rotational speed at an inflow velocity of 3 m/s.

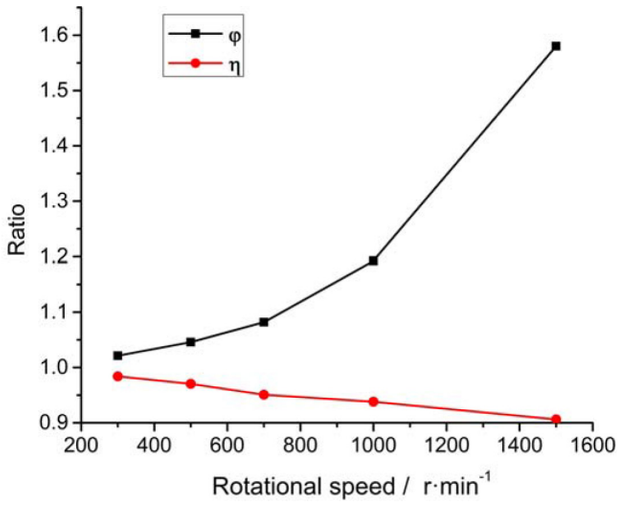

Fig. 8. Pressure exchange performance in different rotational speeds.

most operating conditions. Species transport behavior in the flow field is a joint effect of axial inflow velocity and rotational speed, which affects the resultant velocity, swirl motion, as well as the duration of duct exposure. In our simulation cases of DPE, the relationship between mixing rate and operating conditions shows a monotonic trend.

3.2 Pressure exchange performance

The pressure exchange efficiency of a DPE device can be calculated with Eq. (8):

$$\eta = \frac{P_{so}Q_{so} + P_{bo}Q_{bo}}{P_{si}Q_{si} + P_{bi}Q_{bi}} \tag{8}$$

where P is the static pressure, Q is the flow rate.

Under the balanced operation, the flow rate of high pressure inflow brine equals to the flow rate of low pressure inflow seawater. With the assumption of no leakage, Eq. (8) can be rewritten as,

$$\eta = \frac{P_{so} + P_{bo}}{P_{si} + P_{bi}} \tag{9}$$

As an important feature of DPE in pressure exchange process, liquid pressure can be boosted under the centrifugal force provided by disc rotation. The pressure ratio is defined as:

$$\varphi = \frac{P_{so}}{P_{bi}} \tag{10}$$

Figs. 8 and 9 also reflect the pressure exchange performance of DPE at the steady state in wide-ranging operating conditions. As shown in Fig. 8, pressure transfer efficiency has a negative correlation with rotational speed. When the rotational speed of DPE changes from 300 to 1500 rpm, pressure transfer efficiency decreases from 0.98 to a minimum value of 0.91. Meanwhile, pressure ratio increases to a maximal value of 1.58, which is a result of the increasing centrifugal force.

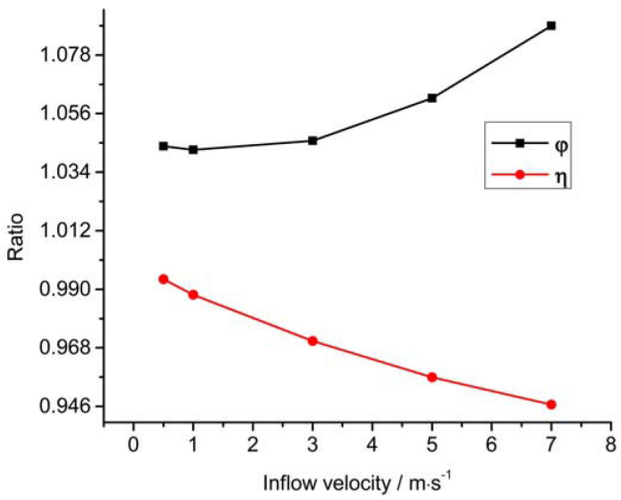

Fig. 9. Pressure exchange performance in different inflow velocities.

In Fig. 9, pressure transfer efficiency has a similar negative correlation with inflow velocity. A difference is observed that the pressure ratio decreases first and then increases with the inflow velocity. This is because a higher velocity will lead to a greater friction loss. When the inflow velocity is much smaller than tangential velocity, the pressure drop will increase with inflow velocity. As the velocity continuously increases, the direction of resultant velocity is closer to duct axis, which contributes to a decline in pressure loss.

It is reported that the pressure drops for the circulation pump to overcome in seawater circulation loops is about 0.3 MPa [15]. Therefore, in a typical RO process at a working pressure of 6 MPa, the pressure ratio of the DPE needs to reach about 1.05 to replace the circulation pump.

3.3. Fields distribution

Fig. 10 illustrates species concentration and pressure distribution field on plane of z/H = 0.5 of DPE at steady stage. The distribution fields are nearly centrosymmetric due to the symmetrical inflow conditions. In Fig. 10a, case B represents for the optimal operating condition with the lowest volumetric mixing rate. The concentrations of Nacl in green areas are 0.048–0.054, which correspond to the mixing rate of 4.3%–6.3%. This range can be regarded as the liquid piston. It is seen that the arrangement of liquid piston is almost circular at a smaller rotational speed for case A, while it becomes oval at a smaller rotational speed when mixing is enhanced. In the most intense mixing case C, the liquid piston appears to be an inverted number 8 and part of the mixing zone flows out of end cover, and this observation is consistent with that suggested in Fig. 6.

Pressure distribution is presented in Fig. 10b. It is seen that the pressure at seawater outlet is higher than high pressure brine inlet. A large pressure gradient is also observed when duct is entering in the sealing zone. This is because that the fluid is suddenly blocked in the sealing zone before the axial velocity becomes zero, generating a pressure surge in the duct end. In comparison, the pressure at a 1500 r/min in Case B is much higher than other cases, this suggests that the rotational speed is a key factor determines the pressure ratio of DPE.

Fig. 11 shows the streamline distributions in high-pressure flow region. Each curve represents for a streamline of a particle released from the HP inlet and the color represents for the velocity magnitude. It is clearly seen that vortex is formed when the duct channel begins to connect to HP outlet, and it gradually dissipates during the rotation. At a

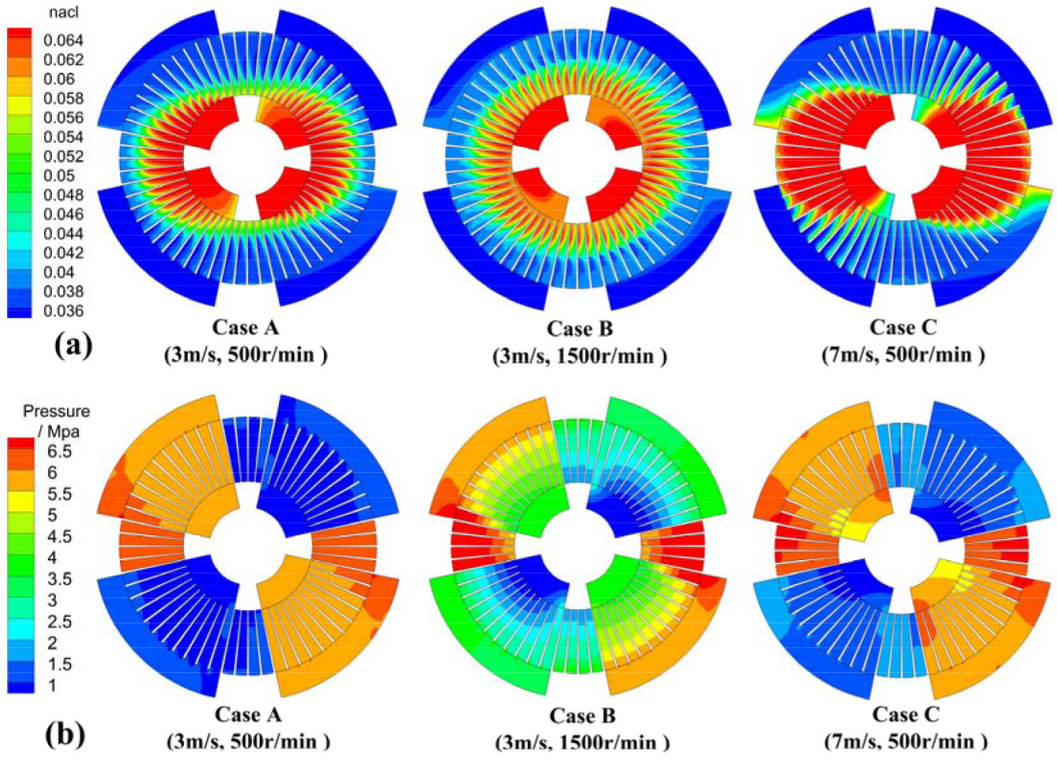

Fig. 10. Fields distribution on plane of z/H = 0.5 of DPE at steady stage, (a) concentration field; (b) pressure field.

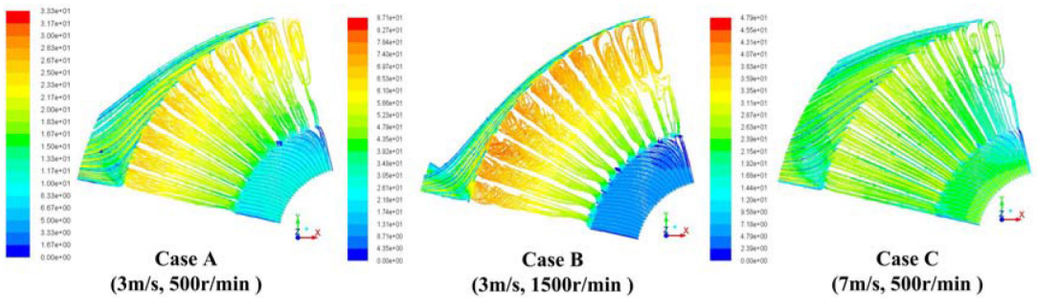

Fig. 11. Streamlines distributionon plane of z/H = 0.5 in high-pressure flow region at steady stage.

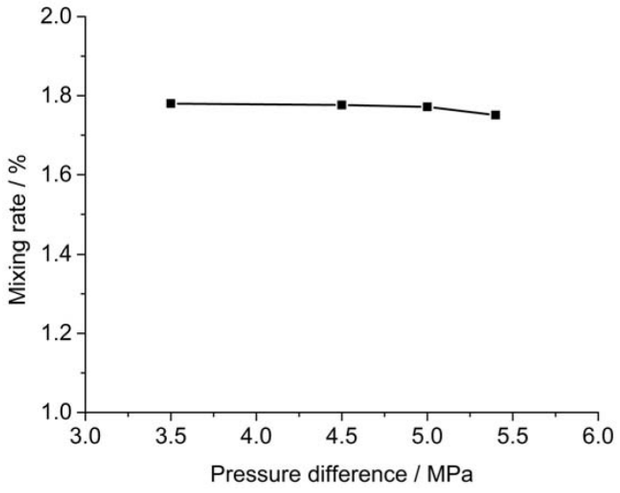

Fig. 12. Volumetric mixing rate varies with pressure difference of inflows.

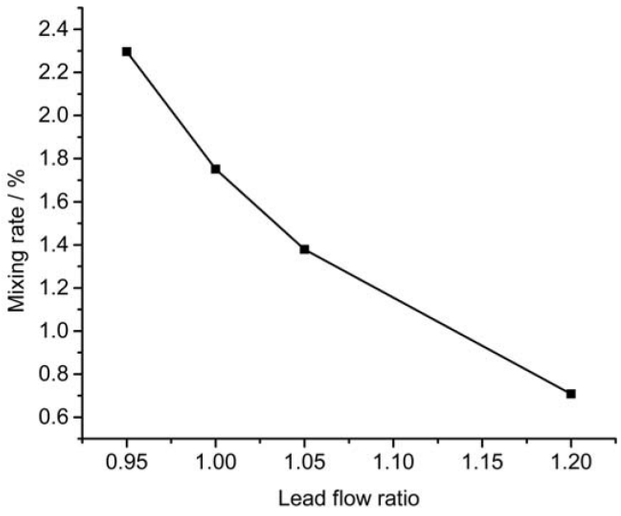

Fig. 13. Volumetric mixing rate varies with lead flow ratio.

higher rotational speed of Case B, the velocity distribution becomes obviously uniform, while for the high inflow velocity of Case C, the streamlines are more straight and parallel.

3.4. Unbalanced operating methods

Most studies for pressure exchanger simulation focuses on its performance in the balanced flow condition. The flow rate of the high-pressure brine inflow equals to that of the low-pressure seawater inflow at balanced flow, and the seawater is pumped to the rotor ducts to discharge the brine at a relatively low pressure.

Apart from the mixing control method by adjusting the rotational speed and inflow velocity, unbalanced effects on the mixing rate are evaluated by increasing the pressure and flowrate of the low-pressure seawater inflow. At such unbalanced flow, pressure difference refers to the pressure of seawater inflow subtracted from the pressure of brine inflow, and the lead flow ratio is defined as the ratio of low-pressure flow rate divided by high-pressure flow rate.

Several unbalanced cases are simulated using the standard case parameters for a reference. Fig. 12 shows the relationship between mixing rate and pressure difference of inflows. It is seen that there is a negligible decline in mixing rate with the increase of pressure differences. The effect of the unbalanced pressure is considered smaller compared with the unbalanced flow rate. As shown in Fig. 13, mixing rate decreases considerably with the increase in flow rate of seawater inflow. A 5% increase of the lead flow ratio results in a 21.3% decrease in mixing rate, thereby it is a considerably efficient method for mixing control.

4. Conclusions

This work presents a novel disc-type pressure exchanger, which combines characteristics of both positive displacement and centrifugal type pressure exchangers. A pressure-boost effect can be achieved by such device to obtain a pressure ratio greater than one. Based on the three-dimensional numerical study of pressure exchange process, the influence of operating parameters on DPE performance was evaluated. Furthermore, unbalanced operating methods were also discussed for mixing control. Simulation results show that mixing rate increases with inflow velocity, while decreases with rotational speed. The pressure transfer efficiency decreases with both of inflow velocity and rotational speed. And the pressure ratio increases with rotating speed while decreases first and then increases with the inflow velocity. Moreover, a 5% increase in the unbalanced flow rate results in an up to 21.3% decrease in mixing rate, suggesting that an unbalanced operating condition can be used for efficient mixing control.

Acknowledgement

This work was supported by the National Natural Science Foundation of China (Grant No. 21376187)

References

[1] A. Farooque, A.T.M. Jamaluddin, A.R. Al-Reweli, P.A.M. Jalaluddin, S.M. Al-Marwani, A.A. Al-Mobayed, A.H. Qasim, Parametric analyses of energy consumption and losses in SWCC SWRO plants utilizing energy recovery devices, Desalination, 219 (2008) 137–159.
[2] A.M. Thomson, Reverse-Osmosis Desalination of Seawater Powered by Photo voltaics Without Batteries, A Doctoral Thesis, Loughborough University, 2003.
[3] R.L. Stover, Development of a fourth generation energy recovery device. A 'CTO's Notebook', Desalination, 165 (2004) 313–321.
[4] L. Yu, Z. Yi-Hui, B. Ming-Shua, 3D numerical simulation on mixing process in ducts of rotary pressure exchanger, Desal. Water Treat., 42 (2012) 269–273.
[5] Y. Zhou, X. Ding, M. Ju, Y. Chang, Numerical simulation on a dynamic mixing process in ducts of a rotary pressure exchanger for SWRO, Desal. Water Treat., 1 (2009) 107–113.
[6] C.C. Mei, Y.H. Liu, A.W.K. Law, Theory of isobaric pressure exchanger for desalination, Desal. Water Treat., 39 (2012) 112–122.

[7] E. Xu, Y. Wang, L. Wu, S. Xu, Y. Wang, S. Wang, Computational fluid dynamics simulation of brine–seawater mixing in a rotary energy recovery device, Ind. Eng. Chem. Res., 53(47) (2014) 18304–18310.
[8] Y. Wang, Y. Duan, J. Zhou, S. Xu, S. Wang, Introducing pre-pressurization/depressurization grooves to diminish flow fluctuations of a rotary energy recovery device: Numerical simulation and validating experiment, Desalination, 413 (2017) 1–9.
[9] Z. Cao, J. Deng, W. Yuan, Z. Chen, Integration of CFD and RTD analysis in flow pattern and mixing behavior of rotary pressure exchanger with extended angle, Desal. Water Treat., 57(33) (2016) 15265–15275.
[10] O.M. Al-Hawaj, The work exchanger for reverse osmosis plants, Desalination, 157(1) (2003) 23–27.
[11] O.M. Al-Hawaj, Theoretical analysis of sliding vane energy recovery device, Desal. Water Treat., 36 (2011) 354–362.
[12] R. Stover, J. Martin, Titan PX-1200 Energy recovery device-test results from the Inima Los Cabos, Mexico, seawater RO facility, Desal. Water Treat., 3 (2009) 179–182.
[13] O.M. Al-Hawaj, The design aspects of rotary work exchanger for SWRO, Desal. Water Treat., 8 (2009) 131–138.
[14] J. Wu, Q. Jin, Y. Wang, P. Tandon, Theoretical analysis and auxiliary experiment of the optimization of energy recovery efficiency of a rotary energy recovery device, Desalination, 415 (2017) 1–7.
[15] B. Peñate, J.A. De la Fuente, M. Barreto, Operation of the RO Kinetic® energy recovery system: Description and real experiences, Desalination, 252 (2010) 179–185.